Generic Phase Curl Localisation for an Individual Identification of Turing-patterned Animals

Tilo Burghardt and Neill Campbell
Department of Computer Science, University of Bristol, MVB, Woodland Rd, BS8 1PY, UK
(mailto:tilo@cs.bristol.ac.uk)

1. Introduction and Overview

A variety of animal species carry permanent markings on their coats, be that for the purpose of survival-boosting camouflage [4, 14] or signalling [5, 8]. In many cases, these prominently visible surface patterns are composed of spots and stripes, which are suspected to originate from reaction-diffusion (RD) systems first described by *Turing* [15]. As a consequence of this deterministic, yet chaotic formation process, resulting markings often differ significantly from individual to individual while following a wider theme typical for a species [11]. Figure 1 illustrates the extent of observable coat variations in two sample species: African penguins and plains zebras.

In this paper we describe minutiae detection in Turing patterns based on the detection of phase curls. The technique compactly captures individuality of RD patterns by robustly localising and typing sparse phase singularities. The foundations of the approach are discussed in detail and we give theoretical and experimental evidence for a generic applicability as a tool for individual animal identification. Finally, we briefly discuss real-world applications that have utilised the technique and can provide extended evaluations.

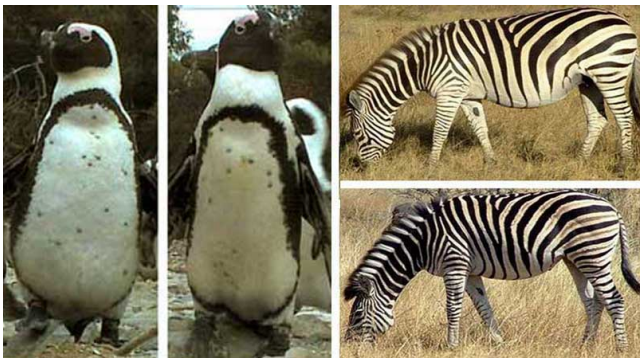

Figure 1: **Coats of African Penguins and Plains Zebras.** The images show two species that develop highly individual markings while following a species-wide, visual theme. Note the unique distributions of line bifurcations on the zebras and of chest spots on the penguins.

2. Properties of Turing-patterned Coats

In order to expose common properties of animal patterns evolving under reaction-diffusion, we first investigate a generic model of animal skin described by a spatiotemporal, two-channel image function $\mathbf{I} : (\mathbf{x}, t) \rightarrow (a, b)$ that maps

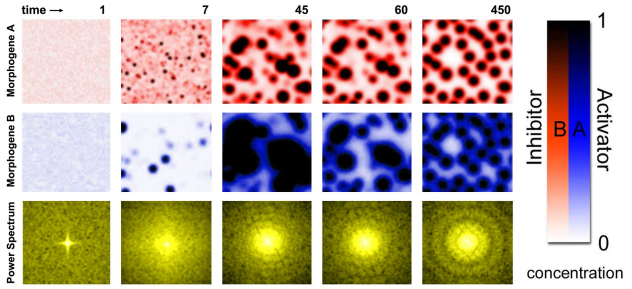

Figure 2: **Evolution of a Reaction-Diffusion System.** Time series of a reaction-diffusion system simulation on a closed 128×128 domain $\mathbf{I}$. Note a transition towards equally sized spots, where the dominant spatial frequency f and its harmonics induce concentric rings in the Fourier spectrum. (parameters: $g_a = \frac{k_1 a^2}{b} - k_2 a + k_1 k_3, g_b = k_4 a^2 - k_5 b + k_6, \gamma = 1, \delta = 10, k_1 = 0.05, k_2 = 0.045, k_3 = k_6 = 0, k_4 = 0.0004, k_5 = 0.2$)

from a position $\mathbf{x}$ on a surface patch and a time t of observation to two local morphogene[1] concentrations a and b. These concentrations are interpreted as facilitators of pigmentation. As outlined by *Murray* [11], the dynamics of such RD systems can be described by the combined effects of morphogene specific reaction kinetics $g_a : (a, b) \rightarrow a$ and $g_b : (a, b) \rightarrow b$, plus continuously changing state diffusion governed by *Fick's Second Law* [6], yielding a partial differential form:

$$\underbrace{d\mathbf{I}/dt}_{dynamics} = \gamma \underbrace{\begin{bmatrix} g_a \\ g_b \end{bmatrix}}_{kinetics} + \begin{bmatrix} 1 & 0 \\ 0 & \delta \end{bmatrix} \underbrace{\nabla^2 \mathbf{I}}_{diffusion} \tag{1}$$

where γ is a scale parameter and δ is the diffusion ratio. Figure 2 visualises an evolution of non-trivial patterns in such a system. According to *Turing's* [15] fundamental finding, non-trivial patterns can evolve on this domain $\mathbf{I}$ if and only if the system converges for $t \rightarrow \infty$ towards a steady state in the absence of diffusion and diverges in its presence. Using linear stability analysis, *Murray* [10] condenses this into four inequations:

$$\begin{gathered} \mathbf{tr}(\mathbf{B}) < 0, |\mathbf{B}| > 0, F > 0, F^2 - 4\delta \cdot |\mathbf{B}| > 0 \\ F = \delta \tfrac{dg_a}{da} + \tfrac{dg_b}{db}, \ \mathbf{B} = \begin{bmatrix} \frac{dg_a}{da} & \frac{dg_a}{db} \\ \frac{dg_b}{da} & \frac{dg_b}{db} \end{bmatrix} \end{gathered} \tag{2}$$

where $\mathbf{B}$ is the Jacobian and F holds a measure for the diffusion-balanced strength of reaction genetics. These constraints circumscribe a compact subspace in the domain of free parameters; the *Turing Space* visualised in Figure 3.

[1] *Turing* [15] employs the term 'morphogenes' (*morphe*=form, *genea*=generation) for the chemicals involved in pattern formation.

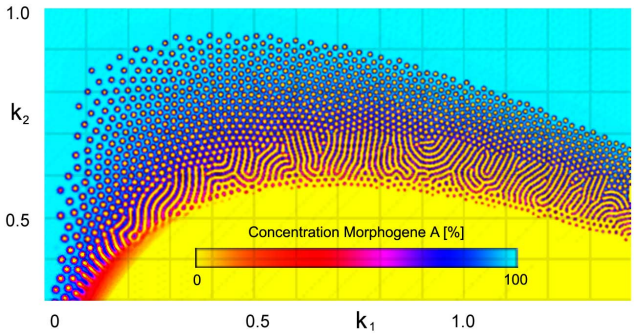

Figure 3: ***Visualisation of the Turing Space.*** The image shows locally occurring patterns superimposed on the pattern-supporting subspace (Turing Space) of the parameter space. [Simulation via Gray-Scott kinetics [9], specifically that is $g_a = k_1(1-a) + ab^2$ and $g_b = b(k_1 + k_2) - ab^2$ under a diffusion ratio of δ=4]

Notice that spot or line patterns in this domain show two system-intrinsic properties:

1) There is a specific *band f of spatial frequencies* that is amplified in Turing patterns. As derived in [11], this dominant band can be described quantitatively as:

$$\gamma L_1/(8\delta\pi^2) < f^2 < \gamma L_2/(8\delta\pi^2) \tag{3}$$

where the $L_{1/2} = F \pm \sqrt{F^2 - 4\delta|\mathbf{B}|}$ represent the two zero crossings of the quadratic dispersion relation. Note that the band is clearly visible in the Fourier spectrum (Figure 2) and that, despite disproportional growth effects *after* pattern fixation (see Figure 4), the band remains widely intact over local regions. Thus, features of Turing patterns are confined in spectral bands around a locally dominant frequency $f_{\mathbf{x}}$, known a priori. This property significantly limits the search space for any practical extraction of local features caused by reaction-diffusion.

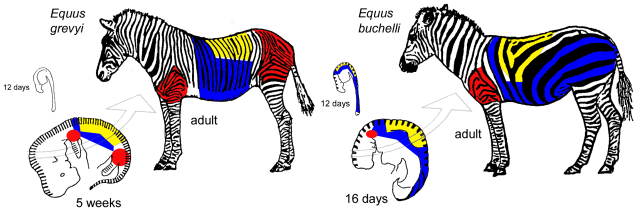

Figure 4: ***Growth-related Differences in Zebra Species.*** Growth after pattern lay-down promotes locally variable dominant pattern frequencies f, while topological variance is strongest in regions at body junctions during lay-down (red) and rapid growth areas (yellow) compared to regions of relative homogeneity (blue). However, in both cases there exists a locally dominant pattern frequency for every location on the coat. [images based on work in [11]]

2) Turing patterns often exhibit *quasi-randomly distributed minutiae points*, more specifically line bifurcations, line endings and isles. As visualised in Figure 5, singularities can be categorised into distinct minutiae types. Amongst other properties, these locations constitute sources or sinks of the local gradient direction field rendering the direction of the gradient structurally indeterministic, i.e. they are phase singularities. Morphologically, they resemble pixels of the skeletonised signal that do not have exactly two neighbours.

Building upon these two properties outlined, we will now describe a generic minutiae detector able robustly to construct a visually characteristic fingerprint for Turing-patterned animals.

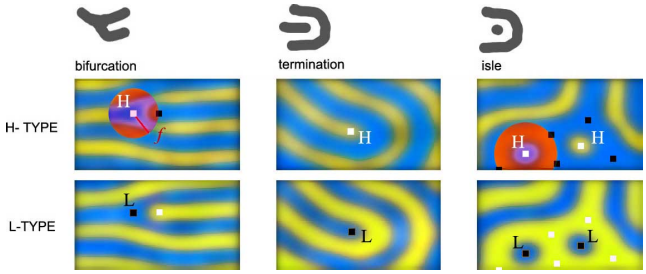

Figure 5: ***Types of Minutiae in Turing Patterns.*** Occurrences in areas of high morphogene concentration (H-type shown as white) and in areas of low concentration (L-type shown as black). Singularities are often accompanied by singularities of opposite type at a distance around the dominant frequency f (indicated as red discs). Three categories can be observed: 1) *bifurcations* where stripes fork, 2) *terminations* where lines end, and 3) *isles* where two terminations have fused into a (symmetrical) spot.

3. Phase Curl Detection

As described, the RD structure of the patterns dictates confining the visual search for minutiae to a spectral band around a locally dominant frequency f, and a strictly local context within the gradient direction field. Starting with a model for the latter, let Θ_f represent the low-pass filtered gradient direction field of the input signal $\mathbf{I}$:

$$\Theta_f = \arctan\left(\frac{\partial G_f * \mathbf{I}}{\partial y}\left(\frac{\partial G_f * \mathbf{I}}{\partial x}\right)^{-1}\right) \tag{4}$$

where $*$ denotes convolution and G_f is a Gaussian low-pass kernel suppressing the redundant spectrum of $\mathbf{I}$ above the locally dominant frequency $f_{\mathbf{x}}$, which is calculated dynamically over local windows in order to adjust for differences in local pattern scale in zebra (see Figure 6a). Vector differentiation $\nabla\Theta_f$ of this field will yield phase singularities at zero crossings as, for instance, shown by *Bray and Wikswo* [1]. However, due to its derivative nature the operator ∇ is sensitive to noise. Since minutiae are surrounded by prominent partial curls of phase as illustrated for an isle-type minutiae landmark in Figure 6b, we suggest utilising the entire structural context of Θ_f around a candidate location $\mathbf{x}$ to probe for minutiae.

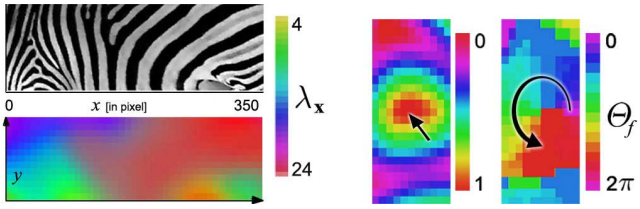

Figure 6: ***Dominant Frequency Field and Gradient Direction Field.*** ***(left)*** Coat pattern patch of a plains zebras and dominant frequency field holding the strongest local frequency $f_{\mathbf{x}}$ at different locations $\mathbf{x}$ of the texture (where the wavelength $\lambda_{\mathbf{x}} = 1/f_{\mathbf{x}}$ is shown in pixels). This field $f_{\mathbf{x}}$ is homogenous in African penguins. ***(right)*** A spatial phase singularity marks extreme point at the centre of an isle feature; the surrounding curl of gradient directions Θ_f;

Curl Detection. In order to test the context of a location $\mathbf{x}$ for a phase curl, a set of m phase histograms $h_{\mathbf{x}}$ is constructed by probing the structure of gradient directions in disc-shaped neighbourhoods. An accumulator array $a(\mathbf{x})$ then gathers evidence from L_2-distances between each n-bin histogram and the even phase distribution (representing an ideal curl). Formally, the calculation of $a(\mathbf{x})$ can be denoted as:

$$a(\mathbf{x}) = 1 - \overbrace{\sum_{j=1}^{m}}^{discs} \sqrt{ w_j \overbrace{\sum_{i=1}^{n}}^{bins} \underbrace{(h^j_{\mathbf{x}}(i) - \overbrace{\frac{|D^j_{\mathbf{x}}|}{n}}^{mean})^2}_{bin\ residual} } \quad (5)$$

where $D^j_{\mathbf{x}}$ is a disc-shaped neighbourhood around $\mathbf{x}$ of radius $j/(2f_{\mathbf{x}}m)$, $\mathrm{h}^j_{\mathbf{x}}(i)$ represents the value of the i^{th} bin and $|D^j_{\mathbf{x}}|/n = \frac{1}{n}\sum_{i=1}^{n} h^j_{\mathbf{x}}(i)$ is the mean bin value of the j^{th} histogram, $|.|$ represents the set cardinality, and w_j is a weighting and normalisation term[2] that favours close-by evidence and ensures that $a(\mathbf{x}) \in (0,1)$. A single bin value is calculated as the number of neighbourhood locations that have their gradient direction falling into the band captured by bin i, that is $h^j_{\mathbf{x}}(i) = \left| \left\{ \mathbf{d} \in D^j_{\mathbf{x}} \mid i = 1 + \lfloor \frac{n\ \Theta_f(\mathbf{d})}{2\pi} \rfloor \right\} \right|$.

This detector is theoretically sound, but basic thresholding of the detector output in real-world examples can produce missing minutiae in cases where the 'single dominant local frequency' constraint degenerates around bifurcations (illustrated in Figure 7).

4. Type and Topology Constraints

The detector $a(\mathbf{x})$ registers both types (represented as L-type=black=-1 and H-type=white=1) of landmarks as distinct maxima. A robust disambiguation between minima and maxima can be achieved by multiplication with a bandpass-sensitive blob response $\mathbf{I}_f$, e.g. using a DoG kernel responding to the dominant band f.

Type Detection. A specific type $T \in \{1, -1\}$ of landmarks (e.g. all L-type features) can then be recognised via a combined detector function $\zeta_T(\mathbf{x})$:

$$\zeta_T(\mathbf{x}) = (\tfrac{T+1}{2} - T\mathbf{I}_f(\mathbf{x}))\ a(\mathbf{x}). \quad (6)$$

Figure 8 illustrates resulting images from an application of $\zeta_T(\mathbf{x})$. The fusion fixes several shortcomings of its constituents: the 'intensity-blindness' of the curl detector is balanced and the poor disambiguation performance of DoG between line endings and line segments due to the radial symmetry of the kernel is eliminated.

Topological Constraint. Finally, based on the observation that minutiae in zebras occur in L-H-type combinations, a topologically-aware detector $t_T(\mathbf{x})$ that can deal with degenerated bifurcations can be constructed as:

$$t_T(\mathbf{x}) = \zeta_T(\mathbf{x})\ \max_{\bar{\mathbf{x}} \in D_{\mathbf{x}}} \left(\zeta_{-T}(\bar{\mathbf{x}})\right) \quad (7)$$

[2]Bin weighting uses $w_j = (M\frac{(1+m-j)}{N_j})^2$ where the normalisation constant $M = \frac{2}{m^2+m}$ balances the importance weights whereas the $N_j = |D^j_{\mathbf{x}}|\sqrt{\frac{(n-1)}{n}}$ describe the maximal cumulative residual of a histogram (i.e. all gradients in $D^j_{\mathbf{x}}$ aim at the same direction). For the implementation, free parameters were chosen to be $m = \lambda_{\mathbf{x}}/2$ (no. of different neighbourhoods) and $n = 8$ (no. of different histogram bins to resolve phase).

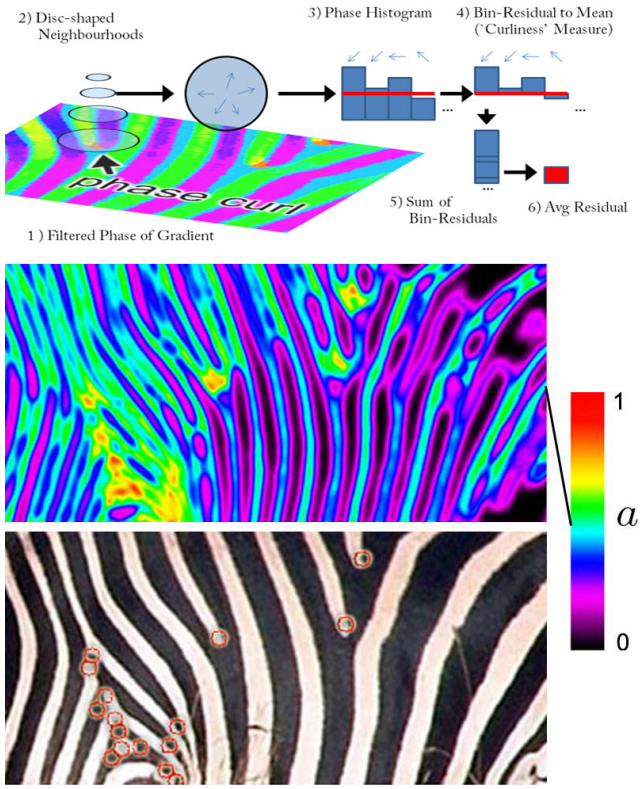

Figure 7: ***Curl Detection by Histogramming.*** ***(top)*** Schematic illustration of the curl detector; ***(middle)*** The image shows a visualisation of the accumulator array $a(\mathbf{x})$ built from ***(bottom)*** the underlying, original zebra texture $\mathbf{I}(\mathbf{x})$ with strong curl maxima superimposed. Note that a number of bifurcation features depart in their properties from the dominant frequency assumption, i.e. the width of contributing stripes varies greatly. As a result, features are missing or misplaced. For instance, the three black bifurcations at the body centre are not detected whilst their counterparts (i.e. white stripe terminations) are found. Topological pairing considerations help overcome the problem of degenerated bifurcations.

where $D_{\mathbf{x}}$ is a disc-shaped neighbourhood[3] around $\mathbf{x}$ of radius $(1+\epsilon)/f_{\mathbf{x}}$.

The technique is robust with respect to noise (see Figure 9 for experimental evidence on penguins). Figure 10 depicts example applications of the typed detector to animal identification from wildlife photographs of African penguins and to plains zebras (using the topological extension).

5. Applications

The technique described has become part of several real-world animal identification systems including the African penguin recognition project (www.SpotThePenguin.com), which provides automated identification of individual African penguins directly in their habitat [12]. Another technique for robustly comparing extracted minutiae landmarks for individual animal identification is, for instance, published and evaluated in [3]. A review of the latest approaches to using extracted landmarks for individual identification against population databases is given in [2]. Recently, a first cross-disciplinary paper of a study comparing

[3]The parameter ϵ is empirically set to 0.5; it embodies the degree of natural deviation of pattern elements from f.

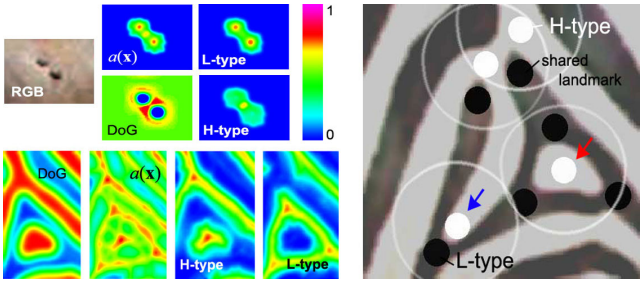

Figure 8: ***Minutiae Type Recognition (left) and Visualisation Topological Constraints (right).***

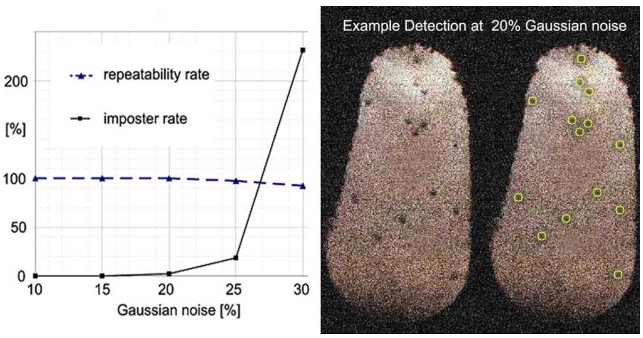

Figure 9: **Repeatability of Spot Detection under Noise.** The graph shows experimental results conducted on 50 penguin chest patterns filmed in good lighting conditions. In order to determine the robustness to noise, Gaussian noise was added at different levels and the percentage of accurately detected spots (repeatability rate) as well as the rate of falsely identified landmarks (imposter rate) were measured.

manual field identification against fully automated penguin identification using the approach (see Figure 10, top) has been published in [12], outlining options for a potentially fully automated population monitoring of African penguins.

6. Conclusion

In this paper, we have presented a technique for minutiae extraction that, underpinned by the theoretical analysis given, is readily applicable to characterising Turing-patterned animal coats. The procedure yields sparse, typed sets of minutiae configurations that are characteristic of individual animals as used in animal ID projects [7, 13, 16], which currently rely on manual landmark identification.

References

[1] M. A. Bray and J. P. Wikswo. Considerations in phase plane analysis for nonstationary reentrant cardiac behavior. *Physical Review E*, 65(5):051902, 2002.

[2] T. Burghardt. *Visual Animal Biometrics*. PhD thesis, University of Bristol, 2008.

[3] T. Burghardt and N. Campbell. Individual animal identification using visual biometrics on deformable coat patterns. In *5th International Conference on Computer Vision Systems (ICVS07)*, 2007. DOI:10.2390.

[4] I. C. Cuthill, M. Stevens, J. Sheppard, T. Maddocks, C. A. Parraga, and T. S. Troscianko. Disruptive coloration and background pattern matching. *Nature*, 434:72–74, 2005.

[5] J. A. Endler. Frequency-dependent predation, crypsis and aposematic coloration. *Philosophical Transactions of the Royal Society of London*, 319:505–522, 1988.

[6] A. Fick. *Philosophical Magazine*, 10(30–39), 1855.

[7] G. Foster, H. Krijger, and S. Bangay. Zebra fingerprints: towards a computer-aided identification system for individual zebra. *African Journal of Ecology*, 45(2):225–227, 2007.

[8] G. Gamberale and B. Tullberg. Evidence for a peak-shift in predator generalization among aposematic prey. In *Biological Sciences*, volume 263, pages 1329–1334, 1996.

[9] P. Gray and S. K. Scott. Sustained oscillations and other exotic patterns of behavior in isothermal reactions. *Journal of Physical Chemistry*, 89:22, 1985.

[10] J. D. Murray. *Mathematical Biology 1 - An Introduction*. Springer-Verlag Berlin Heidelberg, 3rd edition, 2002. ISBN 0-387-95223-3.

[11] J. D. Murray. *Mathematical Biology 2 - Spatial Models and Biomedical Applications*. Springer-Verlag Berlin Heidelberg, 3rd edition, 2003. ISBN 0-387-95228-4.

[12] R. Sherley, T. Burghardt, P. Barham, N. Campbell, and I. Cuthill. Spotting the difference: towards fully-automated population monitoring of african penguins spheniscus demersus. *Endangered Species Research*, 11:101–111, 2010.

[13] C. W. Speed, M. G. Meekan, and C. J. A. Bradshaw. Spot the match - wildlife photo-identification using information theory. *Frontiers in Zoology*, 4(2):1–11, 2007.

[14] M. Stubbs and M. Edmunds. Defence in animals. *The Journal of Animal Ecology*, 45(2):607, 1974.

[15] A. M. Turing. The chemical basis of morphogenesis. In *Philosophical Transactions of the Royal Society of London*, volume B 237. The Royal Society, 1952.

[16] A. M. Van Tienhoven, J. E. Den Hartog, R. A. Reijns, and V. M. Peddemors. A computer-aided program for pattern-matching of natural marks on the spotted raggedtooth shark carcharias taurus. *Applied Ecology*, 44:273–280, 2007.

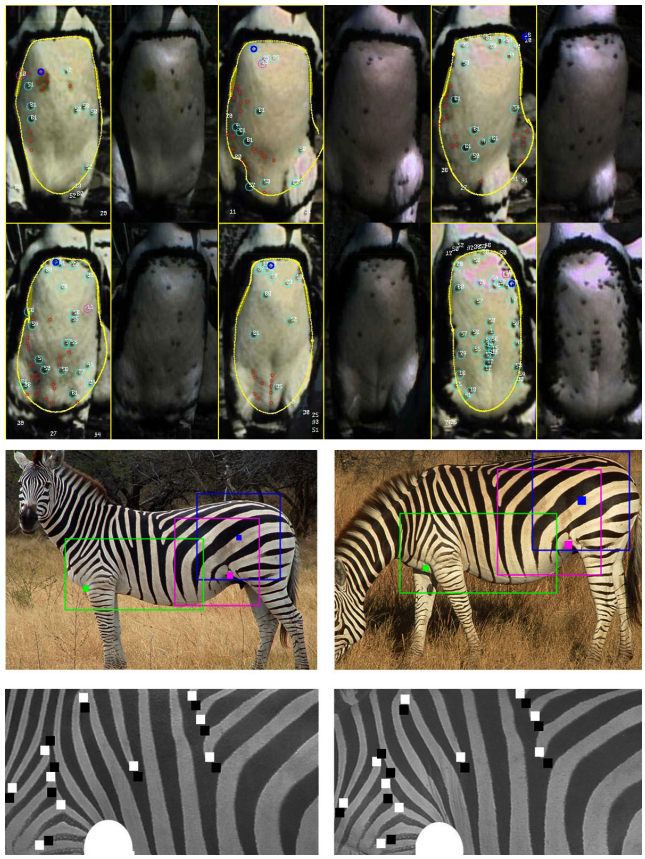

Figure 10: ***Visualisations from Real-world application to penguins and zebras*** (for details please see [12] and [2], respectively)